$$CD_{\mathrm{MinObj}}(X)=\begin{cases}\text{Undefined} & \text{if } \left|N_{\varepsilon\to\infty}(X)\right|<\mathrm{MinObj}\\ \min\limits_{\varepsilon}\left(\left|N_{\varepsilon}(X)\right|\right)\leqslant\mathrm{MinObj} & \text{otherwise.}\end{cases} \tag{14}$$

The reachability distance (*RD*) of object X_p concerning object X_q is defined as the maximum value between the CD of X_q and the distance between the two objects. It is important to note that if the minimum number of objects required for cluster formation, MinObj, exceeds the total number of elements in the set, the reachability distance will be undefined.

$$RD_{\mathrm{MinObj}}(X,X_p)=\begin{cases}\text{Undefined} & \text{if } \left|N_{\varepsilon\to\infty}(X)\right|<\mathrm{MinObj}\\ \max\left(CD_{\mathrm{MinObj}}(X_p),\mathrm{dist}(X,X_p)\right) & \text{otherwise.}\end{cases} \tag{15}$$

The reachability plot is constructed by sequentially evaluating the *RD* between each object and all other objects in the set. In each iteration, the *RD* between the selected object and the remaining objects is computed. This plot serves as a graphical representation of the ordering of objects based on the reachability distance metric facilitating cluster identification of (Boroschek & Bilbao, 2019).

2.2.2 Determination of optimal parameters

The neighborhood size parameter ε must be determined for performing physical mode clustering. The *k*-nearest-neighbor search is used to estimate ε. This search helps in estimating ε by considering the distance of any point *P* to its *k*-th nearest neighbor. Let $D_k(P)$-neighborhood denote the neighborhood surrounding point *P*, which includes its k-nearest neighbors as well. Notably, the $D_k(P)$-neighborhood comprises k+1 points including the point *P* itself. The outline of the estimation algorithm is summarized below:

(1) Determining all the points in its $D_k(P)$-neighborhood.

(2) Accumulating the distances of all points within their respective $D_k(P)$-neighborhoods into a single vector and sorting this vector in ascending order based on the distances.

(3) Plotting the sorted *k*-distance graph, which displays the sorted distances against the corresponding point numbers.

(4) Locating the knee of the curve on the graph where the distance at that particular point serves as an estimate of ε.

The value of ε can be determined using a *k*-distance graph in the mode clustering stage, where the distance to the *k*-nearest-neighbors is plotted in descending order (defined in detail in (Abu Alfeilat et al., 2019; García-Pedrajas et al., 2015)). This graph typically exhibits a multi-linear distribution with a pronounced "elbow" point. The elbow rule refers to the selection of the value at the elbow, which represents an optimal setting for the search distance. It is expected that the k-distance of core points and border points falls within a certain range, while noise points may exhibit much larger *k*-distances. However, in some cases, the knee point may not be visible or there may be multiple knee points, making it difficult to determine. The proposed approach entails calculating the average distance between each point and its *k*-nearest-neighbors method. The value of *k*, which corresponds to Minpts, is specified by the user. These *k*-distances are then shown in ascending order. The objective is to identify the "knee" point, which represents the optimal ε parameter. The knee signifies a threshold where a significant change occurs in the *k*-distance curve. Finally, the determination of the modal parameters that accurately depict the remaining clusters is conducted based on the guidelines proposed in reference (D. Liu et al., 2023), whereby the mean values of $\overline{f}_p$ and $\overline{\xi}_p$ are attributed to each respective cluster. The proposed method enables the estimation of modal participation factors using output-only data through three steps (mode shape extraction, influence vector assumption, and modal participation factor calculation), grounded in classical modal analysis theory (Chopra, 2017; Ewins, 2003).

2.3 Physical mode clustering stage

In this section, the procedure for two-stage automated operational modal identification is presented in Fig. 1. The flowchart of the proposed method is as follows:

(1) The original data measured from practical

engineering should be preprocessed to eliminate the spikes and noise. The block Hankel matrix $\boldsymbol{H}$ is established from the processed data. The observability matrix $\boldsymbol{O}_i$ is estimated based on the singular value decomposition (SVD). Finally, the natural frequency and the damping ratio are identified through $\boldsymbol{A}$ and $\boldsymbol{C}$ deduced from the shifted observability matrix and reversed controllability matrix.

(2) The modal validation criteria (such as HVC, SVC, and UVC) are applied in this step to eliminate spurious modes by Eqs. (1-3, and 10).

(3) The optimal ε is estimated by Eqs. (12-15) based on the KNN method. An enhanced adaptive clustering method is used to identify the physical modes. The means of each cluster are selected as representatives of the physical modes.

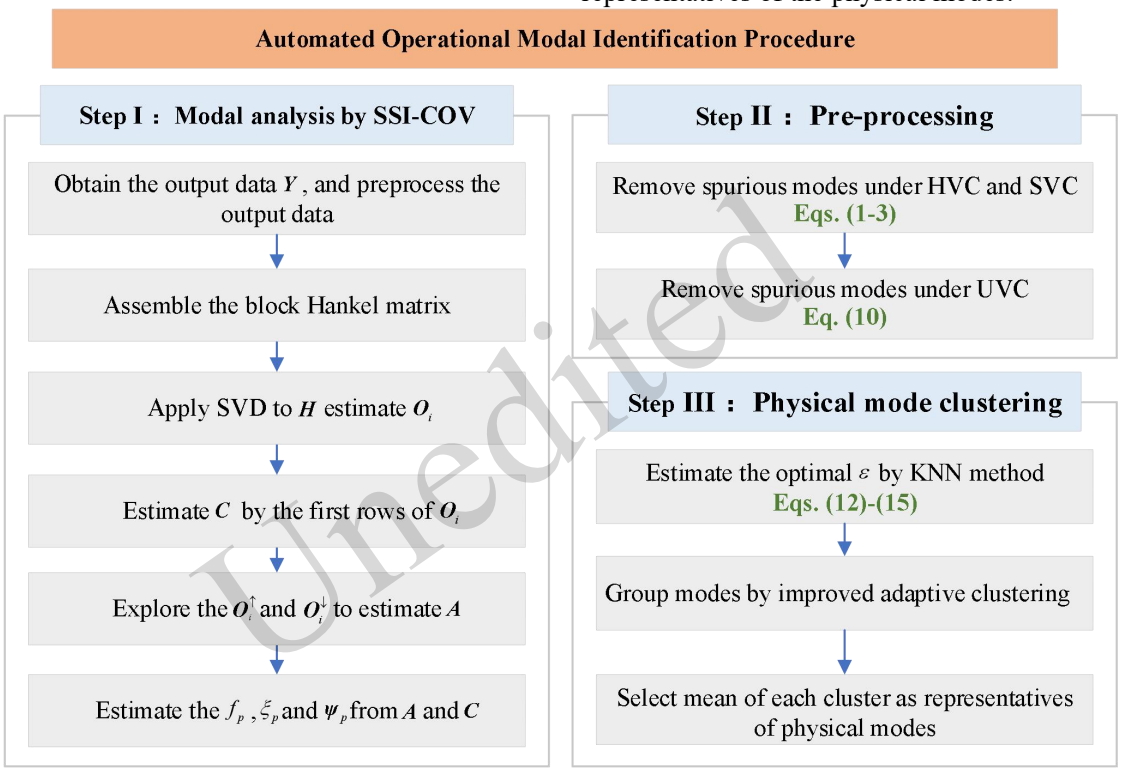

Fig. 1 Flowchart of the two-stage automated operational modal identification

3 Methodology verification and application

3.1 Numerical verification through a ten-story shear frame

3.1.1 Description of the ten-story shear frame

A linear time-invariant ten-story shear frame was used for methodology verification (Fig. 2). The model represents floors as masses m_α ($\alpha \in [1,\cdots,10]$) interconnected by springs k_α and dampers c_α . The matrices of physical parameters (including mass $\boldsymbol{M}$, stiffness $\boldsymbol{K}$, and damping $\boldsymbol{C}$) can be calculated as follows:

$$\boldsymbol{M}=\begin{bmatrix}10 & & & \\ & 10 & & \\ & & \ddots & \\ & & & 10\end{bmatrix},\ \boldsymbol{K}=\begin{bmatrix}2 & -1 & & & \\ -1 & 2 & -1 & & \\ & \ddots & \ddots & \ddots & \\ & & -1 & 1\end{bmatrix}\times 10^4,\ \boldsymbol{C}=\begin{bmatrix}20 & -10 & & & \\ -10 & 20 & -10 & & \\ & \ddots & \ddots & \ddots & \\ & & -10 & 10\end{bmatrix}. \tag{16}$$

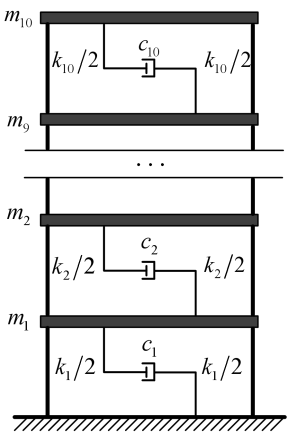

Fig. 2 A schematic diagram of the ten-story shear frame

Each floor is excited by a stationary Gaussian white noise with a mean of 0 to obtain simulated dynamic responses. The excitation lasts 500 s with a sampling frequency of 50 Hz for the requirement of the Nyquist–Shannon sampling theorem. In addition, it is assumed that each floor has an accelerometer arranged at the top of the column for collecting acceleration data. Fig. 3 shows that the signal components exhibit frequency concentration between 2.5 and 10 Hz in the time-frequency transform. The noise content becomes more similar to the physical modes in the higher frequency band making it harder to identify the true physical modes. Consequently, the frequency range of interest for this shear frame was 0-10 Hz. The precomputed parameters of the SSI approach are as follows: i=240, and model order $n \in [12,120]$. Note that a significant challenge encountered by long-term monitoring systems is the possibility of erroneously interpreting these noise frequencies as physical modes.

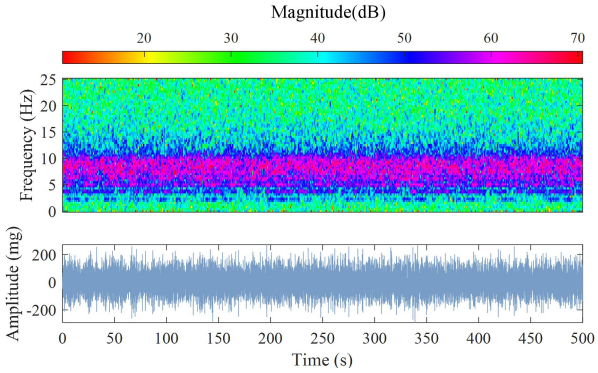

Fig. 3 Results of the time-frequency transform

3.1.2 Identification results

The proposed approach was used to analyze the measured data, as described in Section 2. All calculations were performed on a computer equipped with a 13th Gen Intel(R) Core(TM) i7-13700KF 3.40 GHz and 32 GB of RAM. The same computational setup was used for all subsequent calculations in this study. The computation time for a single run of the proposed method was 156.5 s. The identified results of the spurious modes pre-filtering stage are presented in Fig. 4. Following the application of conventional modal validation criteria, such as the damping ratio check and modal complexity check, all the remaining possible physical modes in the stabilization diagram are shown in Fig. 4(a). The scattered poles of the stabilization diagram are filtered out based on the uncertainty validation criterion in Fig. 4(b). It is evident that, when relying solely on traditional validation criteria, the stabilization diagram still appears chaotic and contains numerous scattered poles. The uncertainty criterion can be used to eliminate spurious modes more efficiently than the usual validation criterion, hence speeding up the automation process. The results of the spurious modes pre-filtering stage show that the uncertainty criterion outperforms the standard validation criterion.

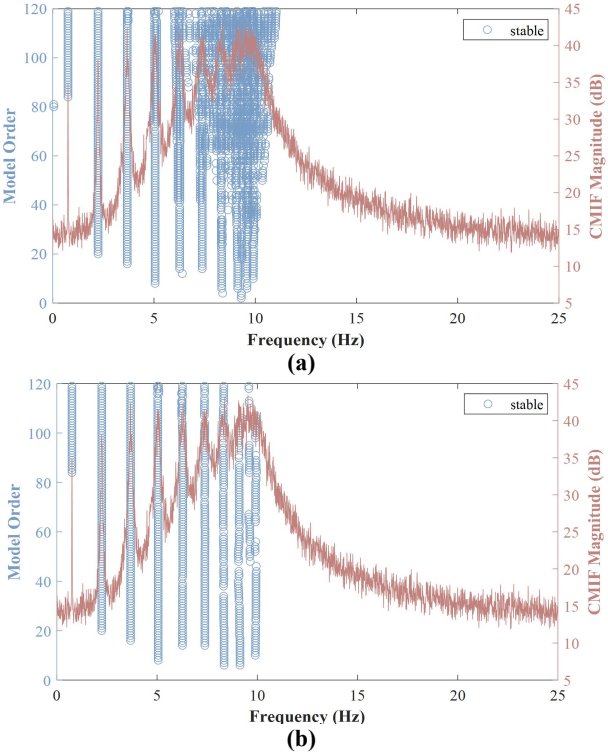

Fig. 4 Modal identification results: (a) after conventional validation criteria; (b) after proposed modal clustering in

Step II

The final step is the automatic detection of clusters from the reachability plot. The reachability plot serves as a graphical representation of the objects' order, obtained through the reachability distance metric. It is derived from the remaining poles in the stabilization diagram following the spurious modes pre-filtering stage. This plot aids in identifying clusters based on the obtained order. By observing the reachability plot, the clustering structure can be observed and derived. As shown in Fig. 5, regions with low reachability distance indicate objects belonging to the same cluster, while regions with high reachability distance are likely to represent outliers. Through a manual inspection, the parameter ε was selected as approximately 0.05.

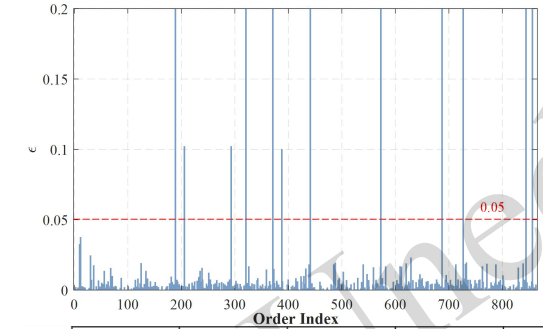

Fig. 5 Reachability plot

To increase automation, Minpts and ε should be set based on the framework of the improved self-adaptive algorithm discussed previously. Fig. 6 shows the estimation of an optimal ε considering optimal values of the k-nearest-neighbors search. The line that joins the curve's initial and final points is defined using this method. The value of ε is defined by the ordinate of the point on the sorted k-dist graph that is perpendicular to and farthest from the line. The algorithm determines the average estimate of ε for each curve when a range of k is given. The distance, which ranges from 0.1 times the number of model orders to the number of model orders (12 to 120), is plotted against the point index k in Fig. 6. The knee of the time-averaged ε occurs at 0.046, which is close to the results of manual inspection. The points over ε are regarded as noise, whereas those below it is part of a cluster.

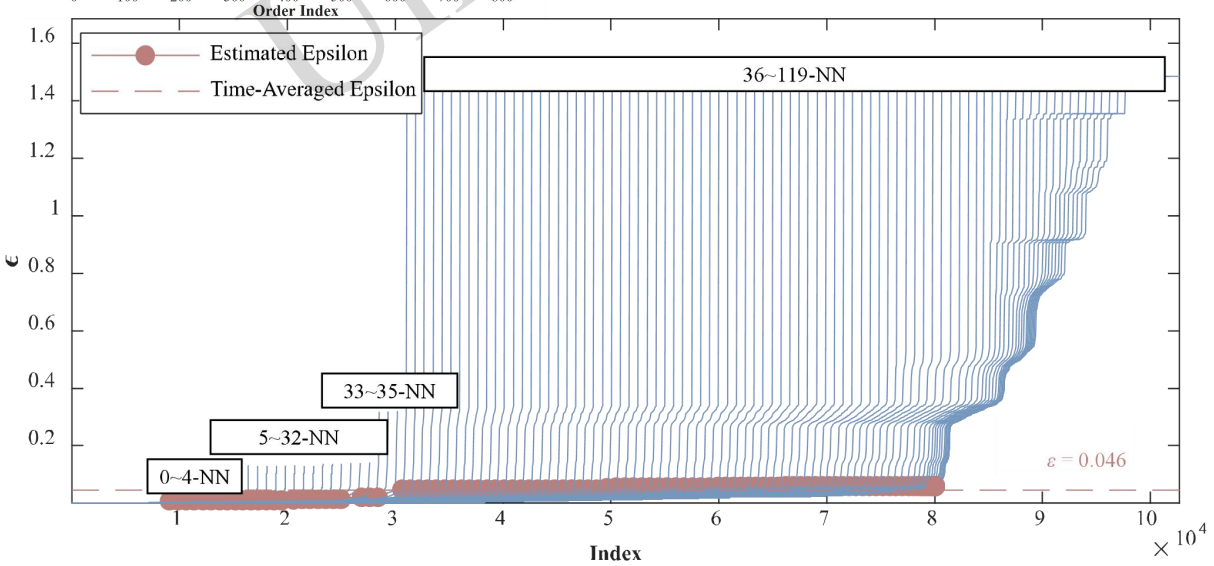

Fig. 6 Determination of Minpts and ε by KNN

Fig. 7 presents the identified results obtained at the modal clustering stage after applying the self-adaptive algorithm. It shows the relationship between damping ratios and frequencies with ten different colors denoting ten distinct groups. The mean values of the identified and theoretical modal parameters are presented by black crosses and red crosses, respectively. The identified damping ratios and frequencies exhibit a close and consistent agreement, indicating the reliability of the results. Table 1 shows the identification results of modal parameters including natural frequencies, damping

ratios, and MAC along with their corresponding theoretical results. The computation of the CV is performed using uncertainty validation criterion analysis, as described in Section 2.1. Note that the proposed AOMA approach effectively captures closely spaced modes from identified frequencies. The closely spaced modes 9.60 and 9.92, are successfully separated. As shown in Fig. 4(a), several spurious closely spaced modes are present in the frequency range from 6 to 10 Hz. The 7th to 10th modes is effectively separated, demonstrating the feasibility of the proposed method in identifying closely spaced modes. Fig. 8 illustrates the identified mode shapes of the structural model under ambient vibration. The identified and theoretical mode shapes are illustrated by red dotted lines and blue solid lines, respectively, while the measured positions are represented by dots. The identified mode shapes are close to the theoretical ones, indicating the effectiveness of the identification process. In conclusion, the proposed approach enables the automatic identification of modal parameters while preserving the physical modes at specific frequencies. The method accurately identifies closely spaced modes without needing to specify the number of clusters or a threshold value for clustering.

Table 1 Proposed AOMA identification results for the ten-story shear frame

Mode	Frequency (Hz)			Damping ratio (%)			MAC
	Identified	CV (%)	Theoretical	Identified	CV (%)	Theoretical	
1	0.7532	0.177	0.7522	0.23	9.483	0.24	0.9953
2	2.2382	0.251	2.2399	0.84	10.064	0.70	0.9997
3	3.6781	0.267	3.6775	1.28	8.851	1.16	0.9994
4	5.0463	0.144	5.0329	1.76	7.436	1.58	0.9995
5	6.2689	0.261	6.2760	1.86	20.85	1.97	0.9996
6	7.3808	0.102	7.3788	2.40	3.395	2.32	0.9989
7	8.3178	0.019	8.3168	2.40	0.744	2.61	0.9994
8	9.0970	0.001	9.0690	2.36	0.003	2.85	0.9995
9	9.6061	0.233	9.6186	2.94	5.168	3.02	0.9976
10	9.9213	0.003	9.9534	3.37	1.273	3.13	0.9938

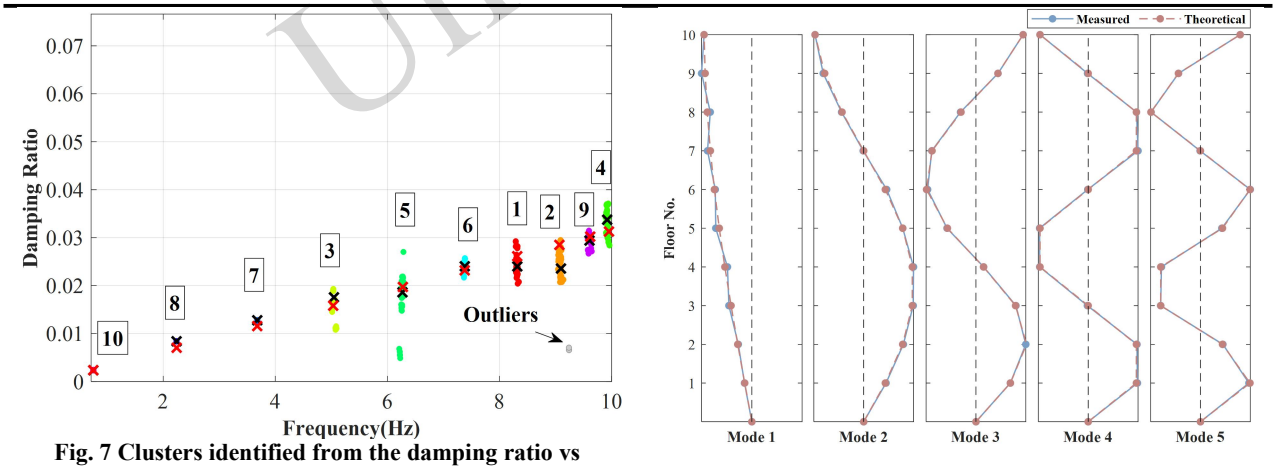

Fig. 7 Clusters identified from the damping ratio vs frequency plot (distinguished by color)

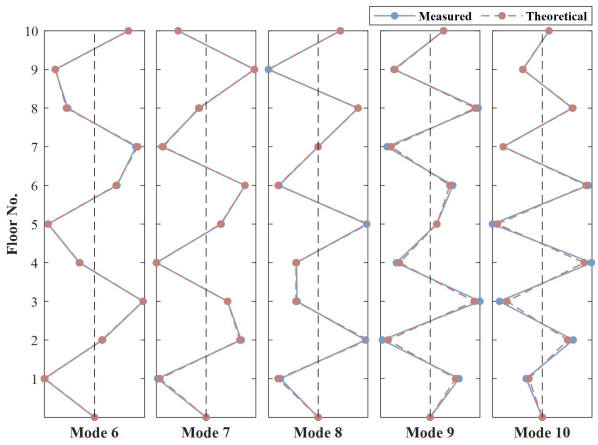

Fig. 8 Comparison between theoretical and measured mode shapes

Due to measurement errors and load uncertainties, noise inevitably contaminates the actual measured acceleration responses. To assess the robustness of the AOMA method, Gaussian white noise at a specified noise level was introduced to the structural acceleration response. The noise level R is defined as follows:

$$\boldsymbol{A}_{noisy} = \boldsymbol{A}_0 + R\boldsymbol{N}\sigma(\boldsymbol{A}_0) \tag{17}$$

where $\boldsymbol{A}_{\text{noisy}}$ denotes the structural acceleration response with added noise, $\boldsymbol{A}_0$ denotes the theoretical structural acceleration response, $\boldsymbol{N}$ denotes the Gaussian white noise sequence with a standard normal distribution of zero mean and unit variance, and $\sigma(\boldsymbol{A}_0)$ denotes the variance of the true structural acceleration response. Considering noise levels ranging from 0% to 5%, the relative deviations of parameter identification results for the frame were calculated. Fig. 8 shows the average relative deviations of the identification results at different noise levels. The curve indicates that the impact of measurement noise on each case is generally consistent. As the noise level increases, the accuracy of the identification results gradually decreases. For different modes, the proposed method provides accurate identification results for natural frequency when the measurement noise is less than 4%, with the average relative deviation for each case not exceeding 5%, demonstrating the robustness of the proposed method against environmental noise.

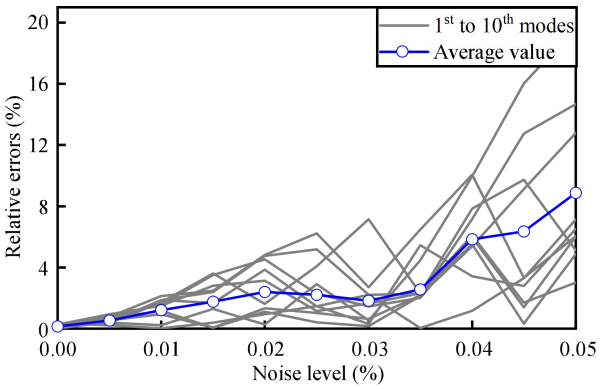

Fig. 9 Relative deviations of parameter identification results under different noise levels

3.2 Application to field measurement of a large-scale bridge

3.2.1 Description of the Taoyaomen Bridge and its monitoring system

Monitoring data from the Taoyaomen Bridge were adopted to further demonstrate the performance of the presented AOMA approach. The Taoyaomen Bridge, a cable-stayed bridge, is located in Zhoushan City, Zhejiang Province, China (Fig. 10). The bridge spans the Taoyaomen waterway and connects Fuchi Island and Cezi Island. It is the third sea-crossing bridge of the Zhoushan mainland-island connection project, with a bridge deck width of 27.6 m and four lanes for two-way traffic. The main girder is a steel structure stiffening girder, and the bridge foundation is drilled piles. The upper part of the bridge is a diamond-shaped tower, with a height of 151 m. Ten accelerometers were strategically installed on the deck for collecting vertical acceleration data under environmental and operational effects (Fig. 10b). The Taoyaomen Bridge is equipped with a structural health monitoring system that consists of a data acquisition transmission system, data management system, and evaluation system (Fig. 10c). The method proposed in this study can be integrated into the evaluation system to analyze real-time monitoring data transmitted over the 4G network, facilitating the automated identification of changes in the bridge's modal parameters. These accelerometers continuously recorded the vibrations at a sampling frequency of 50 Hz. The acceleration data used in this study were collected on 7 July, 2022, at 3:00 p.m. A dataset with a length of 15,000 samples was selected for estimating the modal parameters. The parameters

of the SSI-COV algorithm are set as follows: the model order ranged from 6 to 60, and i = 120. The computation time for a single run of the proposed method was 126.5 s.

(a)

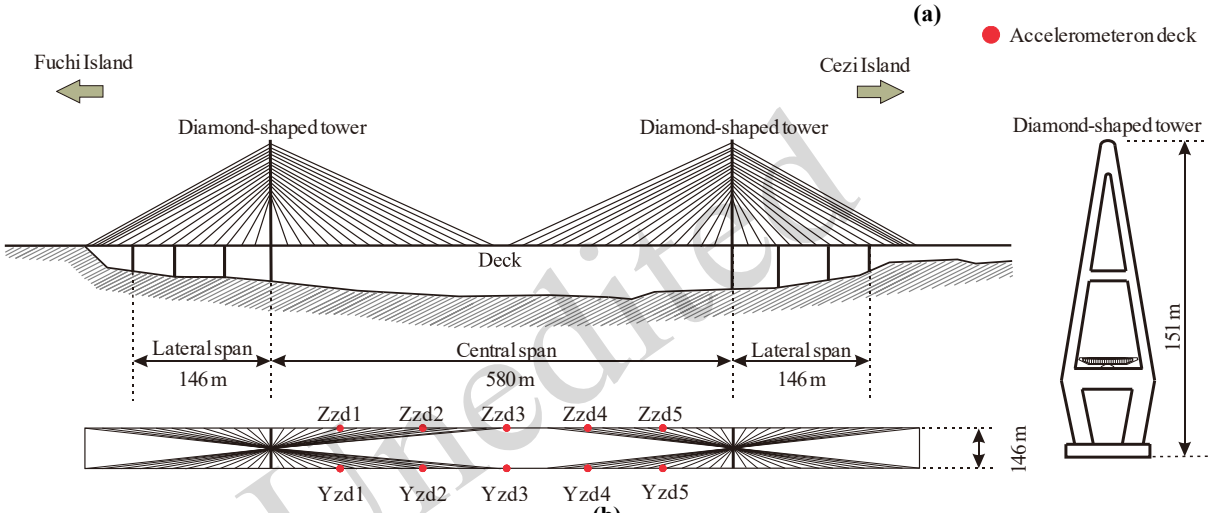

(b)

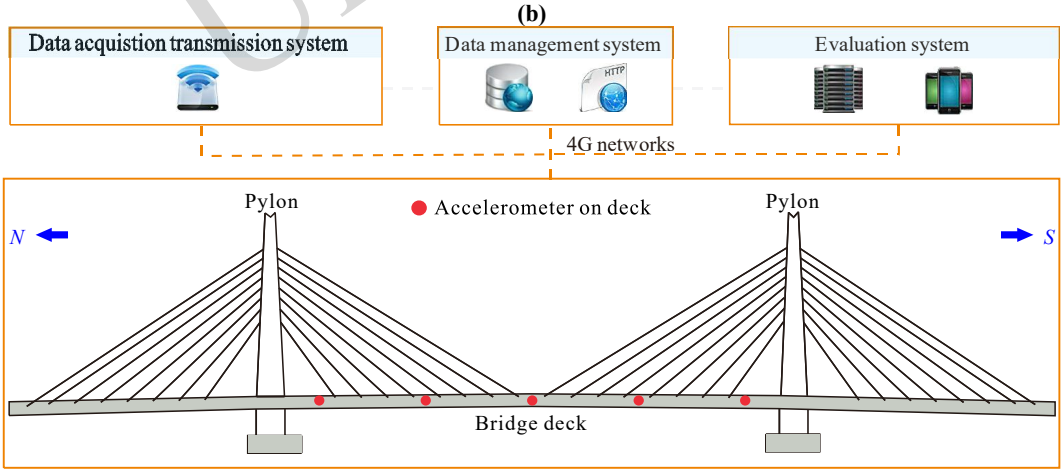

(c)

Fig. 10 Description of the Taoyaomen bridge: (a) photo; (b) geometry and layout of the sensors; (c) monitoring system

3.2.2 Identification results

The identification results obtained with traditional validation criteria are shown in Fig. 11(a), where many spurious modes are present. The singular value spectrum is illustrated in the stabilization diagram. The conventional and uncertainty validation criteria were applied to improve the clarity of the diagram (Fig. 11b). The inset box in Fig. 11(b) shows the identification of nine vertical blue alignments while the conventional stabilization diagram still looks busy. This scattering indicates the presence of spurious mode 3.5 Hz indicating the significant influence of environmental changes on the high-order mode fluctuations. The identification results of Stage Ⅱ show that the uncertainty criterion works better

than conventional validation criteria. Accurate assessment of these fluctuations is essential for any AOMA approach, regardless of its particular application.

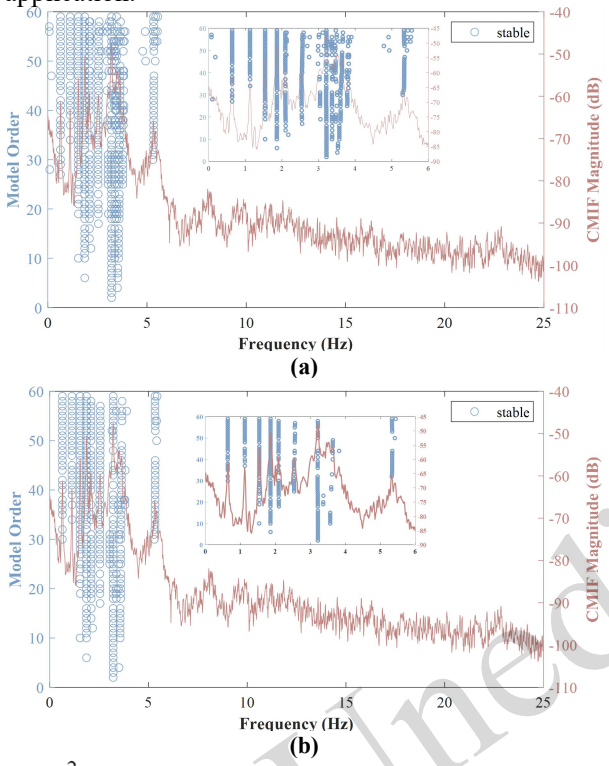

Fig. 11 Modal identification results: (a) after conventional validation criteria; (b) after proposed modal clustering in Stage II

The evolution of the natural frequencies of the first six modes is plotted. The physical modes are clustered using OPTICS combined with the KNN algorithm. The physical mode clustering step then begins with an estimated clustering threshold. The estimated threshold in this case was 0.193 (Fig. 12). This threshold represents a stricter criterion that enables the removal of more spurious modes while preserving the physical modes. The first nine modes, labeled as modes 1 to 9 (a total of nine clusters), were used as a baseline in Fig. 13. Note that modes 4 and 5 have close spacing, which is a prevalent problem in AOMA. To address this issue, robust outlier identification was used to eliminate extremely variable frequencies and damping ratios. The relationship between damping ratios and frequencies is illustrated in Fig. 13. Each of the nine different colors represents a distinct cluster, where the black crosses indicate the mean damping ratio. The results are more reliable because of the strong agreement and consistency between the identified damping ratios and natural frequencies.

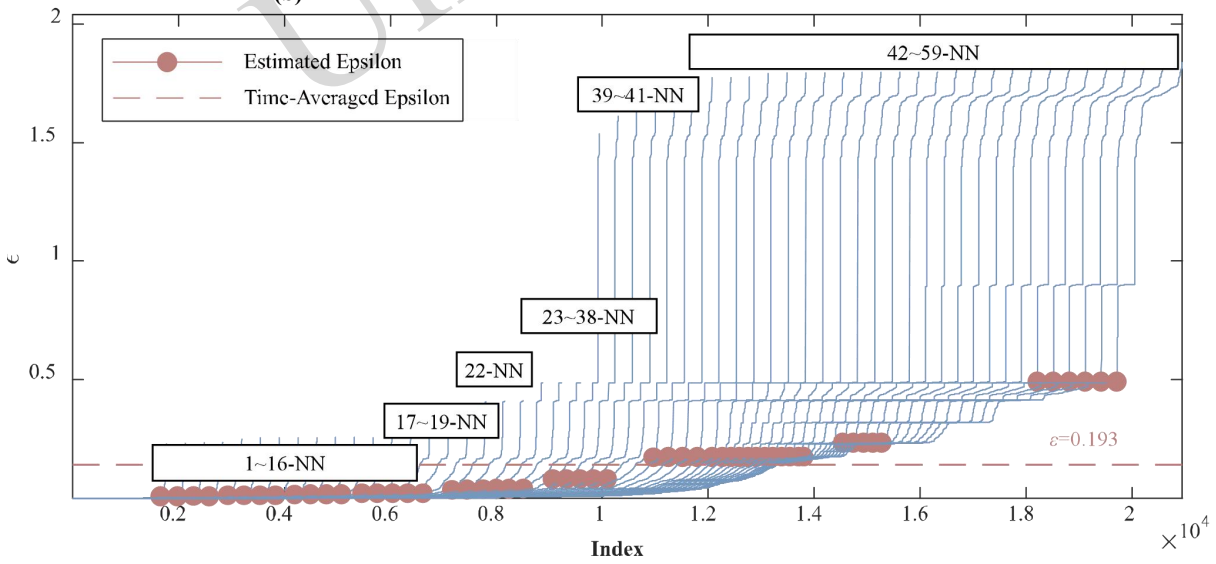

Fig. 12 Determination of Minpts and ε by KNN

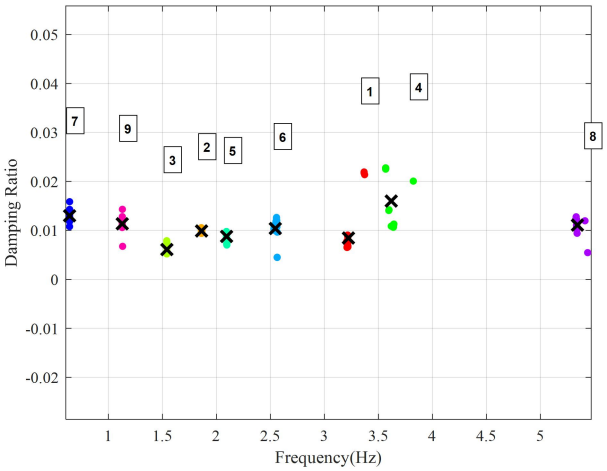

Fig. 13. Clusters identified from the damping ratio vs frequency plot (distinguished by color)

The distribution of identified frequencies and damping ratios of the first six mode shapes for 96 datasets for 2 days are shown in Figs. 14-15. All natural frequencies of the first six modes fit well with Gaussian normal distributions. On the other hand, the damping ratios show a heavily-tailed Weibull distribution. The identification results indicate that modal parameter identification is significantly affected by changes in the environment. In conclusion, the proposed two-stage AOMA technique performed remarkably well in modal parameter tracking over 96 observed datasets during two days without the need for human intervention. The results of this study show that the proposed AOMA approach is promising, robust, and applicable for online structural health monitoring with potential extension to different types of structures.

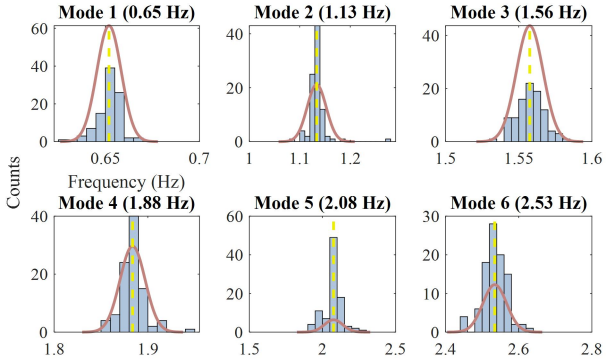

Fig. 14 Frequency distributions (normal distribution)

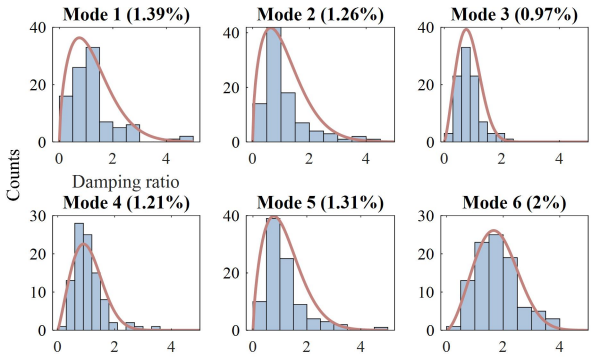

Fig. 15 Damping ratio distributions (Weibull distribution)

The mode shapes identified from measured data and FEM analysis were compared to assess the identification accuracy of the proposed AOMA approach. Fig. 16 shows the first six normalized mode shapes of the Taoyaomen Bridge. The blue lines are the nodes of the bridge deck and the red dots are the positions of the accelerometers. The first, second, and fifth modes are the flexural modes in the vertical direction. The third, fourth, and sixth modes are the torsional modes. The accuracy of the identified modal parameters meets engineering requirements, as shown by the average MAC of the mode shapes in AMOA and FEM analysis being greater than 0.95. Because of the influence of environmental noise, the MAC of high-order mode shapes is slightly lower than that of low-order mode shapes.

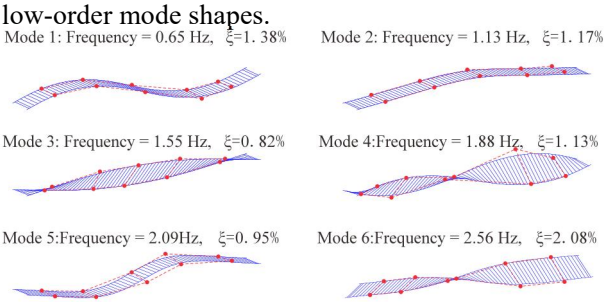

Fig. 16 The first six normalized mode shapes of the Taoyaomen Bridge

The proposed AOMA approach was used to identify the modal parameters continually. The results of the natural frequencies identified for the first six mode shapes are shown in Fig. 17. The proposed approach had a high accuracy in the continuous automatic identification of modal parameters. The identified natural frequencies did not seem to be sensitive to the environmental effects. The damping ratio is another important modal parameter, which is important for vibration control of the large-span structures. The time histories of damping ratios are shown in Fig. 18. Although more spread than the natural frequencies, all of the measured damping

ratios maintained a respectable fluctuation amplitude. Sudden peaks can be observed for the 1st, 2nd, and 5th mode shapes. According to the recorded data from the anemometer at the bridge site, sudden wind gusts during this period may have induced a large amplitude spike in the damping ratios.

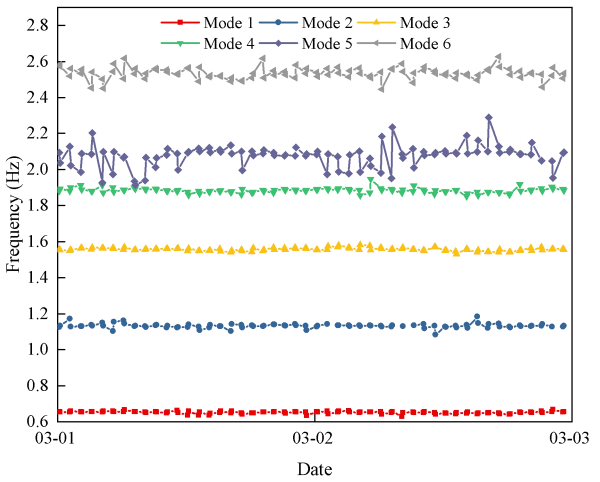

Fig. 17 Identified natural frequencies of the first six modes

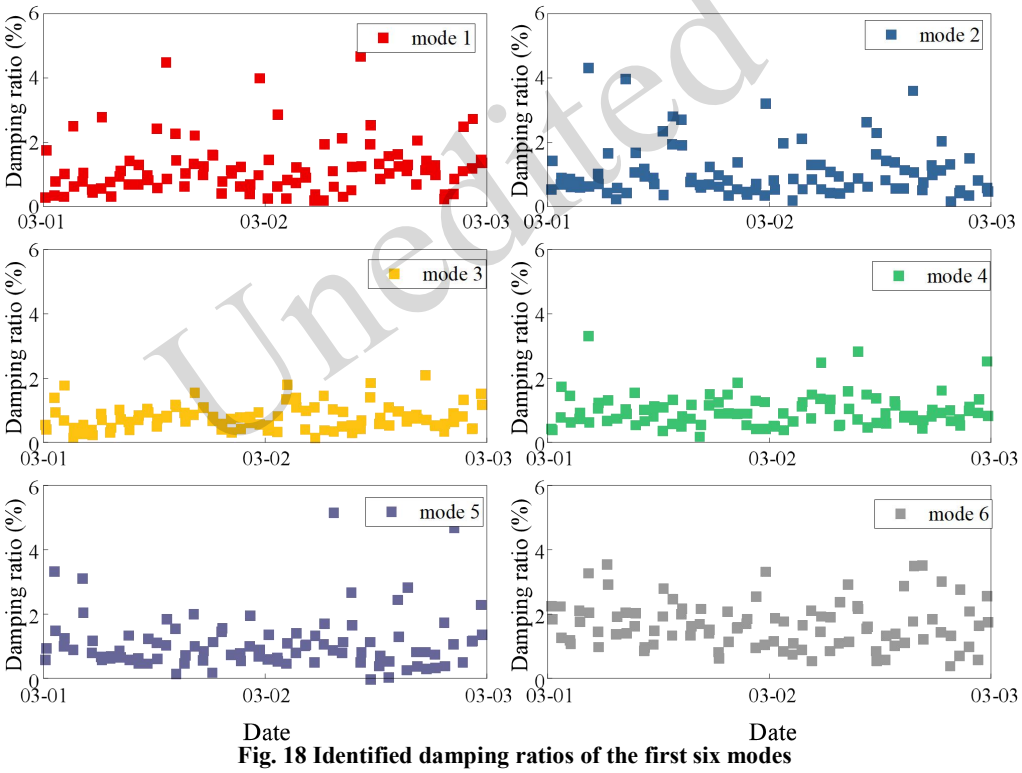

Fig. 18 Identified damping ratios of the first six modes

4 Conclusions

In this paper, we present a new two-stage framework for AOMA based on Ordering Points to Identify the Clustering Structure (OPTICS). The distinctive feature of this framework is the incorporation of a fully automatic density-based clustering approach without requiring specification of the number of clusters in advance. The effectiveness and applicability of the proposed approach are demonstrated through numerical verification on a ten-story shear frame and practical application to the Taoyaomen Bridge. The main summaries and conclusions are as follows:

1. According to the results of the modal parameters identified from the ten-story frame and the Taoyaomen Bridge, the frequencies and damping ratios of each mode remain within a narrow range, validating that the proposed approach can effectively remove spurious modes and identify physical modes.

2. The proposed approach performs well in identifying closely spaced modes, as demonstrated by

numerical verification on the shear frame. These modes have been successfully discovered without the need for specifying the number of clusters or a threshold value for clustering.

3. Six mode shapes of the Taoyaomen Bridge were identified, and the modal parameters were continuously tracked over several days. The analysis of extensive datasets collected from SHM systems confirmed the practicability of the approach.

Acknowledgments

This work was supported by the National Natural Science Foundation of China (52408200), Natural Science Foundation of Jiangsu Province (BK20240996), Suzhou Science and Technology Plan (Basic Research) Project (SJC2023002), and Natural Science Research Projects of Colleges and Universities in Jiangsu Province (24KJB560022).

Author contributions

Yi CHEN and Wenwei FU designed the research and wrote the first draft of the manuscript. Hui YANG supervised and administrated the project. Shi-Ying WANG helped to organize the manuscript. Yaozhi LUO and Yanbin SHEN revised and edited the final version.

Conflict of interest

Yi CHEN, Wenwei FU, Yaozhi LUO, Yanbin SHEN, Hui YANG, and Shi-Ying WANG declare that they have no conflict of interest.

References

Abu Alfeilat HA, Hassanat ABA, Lasassmeh O, et al., 2019. Effects of Distance Measure Choice on K-Nearest Neighbor Classifier Performance: A Review. *Big Data*, 7(4), 221–248. https://doi.org/10.1089/big.2018.0175

Boroschek RL, and Bilbao JA, 2019. Interpretation of stabilization diagrams using density-based clustering algorithm. *Engineering Structures*, 178, 245–257. https://doi.org/10.1016/j.engstruct.2018.09.091

Cabboi, A, Magalhães F, Gentile C, and Cunha Á, 2017. Automated modal identification and tracking: Application to an iron arch bridge. Structural Control and Health Monitoring, 24(1), e1854.

Chen J, Xu YL, and Zhang RC, 2004. Modal parameter identification of Tsing Ma suspension bridge under Typhoon Victor: EMD-HT method. *Journal of Wind Engineering and Industrial Aerodynamics*, 92(10), 805–827. https://doi.org/10.1016/j.jweia.2004.04.003

Chopra A, 2017. Dynamics of Structures-Theory and Applications to Earthquake Engineering.

Civera M, Mugnaini V, and Zanotti Fragonara L, 2022. Machine learning-based automatic operational modal analysis: A structural health monitoring application to masonry arch bridges. *Structural Control and Health Monitoring*, 1–23. https://doi.org/10.1002/stc.3028

Civera M, Sibille L, Zanotti Fragonara L, et al., 2023. A DBSCAN-based automated operational modal analysis algorithm for bridge monitoring. *Measurement*, 208, 112451. https://doi.org/10.1016/j.measurement.2023.112451

Desjardins S, and Lau D, 2022. Advances in intelligent long-term vibration-based structural health-monitoring systems for bridges. *Advances in Structural Engineering*, 25(7), 1413–1430. https://doi.org/10.1177/1369433222

Döhler M., and Mevel L, 2013. Efficient multi-order uncertainty computation for stochastic subspace identification. *Mechanical Systems and Signal Processing*, 38(2), 346–366. https://doi.org/10.1016/j.ymssp.2013.01.012

Doroudi R, Hosseini Lavassani SH, Shahrouzi M, et al., 2022. Identifying the dynamic characteristics of super tall buildings by multivariate empirical mode decomposition. *Structural Control and Health Monitoring*, 29(11). https://doi.org/10.1002/stc.3075

Ereiz S, Duvnjak I, and Fernando Jiménez-Alonso J, 2022. Review of finite element model updating methods for structural applications. *Structures*, 41, 684–723. https://doi.org/10.1016/j.istruc.2022.05.041

Ewins DJ, 2003. Modal Testing, Theory, Practice and Application. *Reinforced Plastics*, 47(4), 38–43.

Fan G, Li J, and Hao H, 2019. Improved automated operational modal identification of structures based on clustering. *Structural Control and Health Monitoring*, 26(12), 1–23. https://doi.org/10.1002/stc.2450

Farrar CR., and Worden K, 2007. An introduction to structural health monitoring. *Philosophical Transactions of the Royal Society A: Mathematical, Physical and Engineering Sciences*, 365(1851), 303–315. https://doi.org/10.1098/rsta.2006.1928

Feng Y, Su Y, Zhao C, et al., 2024. A two-stage automated OMA framework for transmission towers based on clustering algorithms. *Structures*, 61, 106023. https://doi.org/10.1016/j.istruc.2024.106023

García-Pedrajas N, Del Castillo JAR, and Cerruela-García G, 2015. A proposal for local k values for k-nearest neighbor rule. *IEEE Transactions on Neural Networks and Learning Systems*, 28(2), 470–475.

Garcia-Perez A, Amezquita-Sanchez, JP, Dominguez-Gonzalez, A, et al., 2013. Fused empirical mode decomposition and wavelets for locating combined damage in a truss-type structure through vibration analysis. *Journal of Zhejiang University-SCIENCE A (Applied Physics & Engineering)*, 14(9), 615–630. https://doi.org/10.1631/jzus.A1300030

Greś S, Döhler M, Andersen P, and Mevel, L, 2021. Uncertainty quantification for the Modal Phase Collinearity of complex mode shapes. *Mechanical Systems and Signal Processing*, 152, 107436. https://doi.org/10.1016/j.ymssp.2020.107436

Gu J, Gul M, and Wu X, 2017. Damage detection under varying temperature using artificial neural networks.

Structural Control and Health Monitoring, 24(11), e1998. https://doi.org/10.1002/stc.1998

He M, Liang P, Li J, et al., 2021. Fully automated precise operational modal identification. *Engineering Structures*, 234, 111988. https://doi.org/10.1016/j.engstruct.2021.111988

He Y, Yang JP, and Li YF, 2022. A three-stage automated modal identification framework for bridge parameters based on frequency uncertainty and density clustering. *Engineering Structures*, 255, 113891. https://doi.org/10.1016/j.engstruct.2022.113891

Hou R, and Xia Y, 2021. Review on the new development of vibration-based damage identification for civil engineering structures : 2010 – 2019. *Journal of Sound and Vibration*, 491, 115741. https://doi.org/10.1016/j.jsv.2020.115741

Huang CS, Le QT, Su WC, et al., 2020. Wavelet-based approach of time series model for modal identification of a bridge with incomplete input. *Computer-Aided Civil and Infrastructure Engineering*, 35(9), 947–964. https://doi.org/10.1111/mice.12539

Jeong S, Ferguson M, Hou R, et al., 2019. Sensor data reconstruction using bidirectional recurrent neural network with application to bridge monitoring. *Advanced Engineering Informatics*, 42, 100991. https://doi.org/10.1016/j.aei.2019.100991

Jin SS, Jeong S, Sim SH, et al., 2021. Fully automated peak-picking method for an autonomous stay-cable monitoring system in cable-stayed bridges. *Automation in Construction*, 126, 103628. https://doi.org/10.1016/j.autcon.2021.103628

Kang F, and Li J, 2020. Displacement Model for Concrete Dam Safety Monitoring via Gaussian Process Regression Considering Extreme Air Temperature. *Journal of Structural Engineering*, 146(1), 05019001. https://doi.org/10.1061/(asce)st.1943-541x.0002467

Liu D, Bao Y, and Li H, 2023. Machine learning-based stochastic subspace identification method for structural modal parameters. *Engineering Structures*, 274, 115178. https://doi.org/10.1016/j.engstruct.2022.115178

Liu YC, Loh CH, and Ni YQ, 2013. Stochastic subspace identification for output-only modal analysis: application to super high-rise tower under abnormal loading condition. *Earthquake Engineering & Structural Dynamics*, 42(4), 477–498. https://doi.org/10.1002/eqe.2223

Luo Y, Fu W, Wan HP, and Shen Y, 2022. Load-Effect Separation of a Large-Span Prestressed Structure Based on an Enhanced EEMD-ICA Methodology. *Journal of Structural Engineering*, 148(3), 4021288. https://doi.org/10.1061/(ASCE)ST.1943-541X.0003263

Luo YZ, Chen Y, Wan HP, et al., 2021. Development of laser-based displacement monitoring system and its application to large-scale spatial structures. *Journal of Civil Structural Health Monitoring*, 11(2), 381–395. https://doi.org/10.1007/s13349-020-00459-4

Mao JX, Wang H, Fu YG, et al., 2019. Automated modal identification using principal component and cluster analysis: Application to a long-span cable-stayed bridge. *Structural Control and Health Monitoring*, 26(10), 1–20. https://doi.org/10.1002/stc.2430

McLachlan GJ, Lee SX, and Rathnayake SI, 2019. Finite mixture models. *Annual Review of Statistics and Its Application*, 6(1988), 355–378. https://doi.org/10.1146/annurev-statistics-031017-100325

Mostafaei H, Ghamami M, and Aghabozorgi P, 2021. Modal identification of concrete arch dam by fully automated operational modal identification. *Structures*, 32, 228–236. https://doi.org/10.1016/j.istruc.2021.03.028

Mugnaini V, Zanotti FL, and Civera M, 2022. A machine learning approach for automatic operational modal analysis. *Mechanical Systems and Signal Processing*, 170, 108813. https://doi.org/10.1016/j.ymssp.2022.108813

Neu E, Janser F, Khatibi AA, et al., 2017. Fully Automated Operational Modal Analysis using multi-stage clustering. *Mechanical Systems and Signal Processing*, 84, 308–323. https://doi.org/10.1016/j.ymssp.2016.07.031

Ni YQ, Wang YW, and Zhang C, 2020. A Bayesian approach for condition assessment and damage alarm of bridge expansion joints using long-term structural health monitoring data. *Engineering Structures*, 212, 110520.

Pan Y, Ventura CE, Xiong H, et al., 2020. Model updating and seismic response of a super tall building in Shanghai. *Computers and Structures*, 239, 106285. https://doi.org/10.1016/j.compstruc.2020.106285

Peeters B, and De RG, 1999. Reference-based stochastic subspace identification for output-only modal analysis. *Mechanical Systems and Signal Processing*, 13(6), 855–878. https://doi.org/10.1006/mssp.1999.1249

Peeters B, and Lowet G, 2004. A New Procedure for Modal Parameter Estimation. *Journal of Sound and Vibration*, 38(1), 24–29.

Rainieri C, and Fabbrocino G, 2014. Operational modal analysis of civil engineering structures. In Springer, New York. Springer.

Ran L, Ding Y, Chen Q, et al., 2023. Influence of adjacent shield tunneling construction on existing tunnel settlement: field monitoring and intelligent prediction. *Journal of Zhejiang University-SCIENCE A (Applied Physics & Engineering)*, 24(12), 1106–1119. https://doi.org/10.1631/jzus.A2200573

Ren WX, and Zong ZH, 2004. Output-only modal parameter identification of civil engineering structures. *Structural Engineering and Mechanics*, 17(3–4), 429–444. https://doi.org/10.12989/SEM.2004.17.3_4.429

Reynders E, Maes K, Lombaert G, et al., 2016. Uncertainty quantification in operational modal analysis with stochastic subspace identification: Validation and applications. *Mechanical Systems and Signal Processing*, 66–67, 13–30. https://doi.org/10.1016/j.ymssp.2015.04.018

Reynders E, Pintelon R, and De Roeck G, 2008. Uncertainty

bounds on modal parameters obtained from stochastic subspace identification. *Mechanical Systems and Signal Processing*, 22(4), 948–969. https://doi.org/10.1016/j.ymssp.2007.10.009

Reynders E, and Roeck GD, 2008. Reference-based combined deterministic–stochastic subspace identification for experimental and operational modal analysis. *Mechanical Systems and Signal Processing*, 22(3), 617–637. https://doi.org/10.1016/j.ymssp.2007.09.004

Sadeqi A, Esfandiari A, Sanayei M, et al., 2022. Automated operational modal analysis based on long-term records: A case study of Milad Tower structural health monitoring. *Structural Control and Health Monitoring*, 29(10), e3037. https://doi.org/10.1002/stc.3037

Saxena A, Prasad M, Gupta A, et al., 2017. A review of clustering techniques and developments. *Neurocomputing*, 267, 664–681. https://doi.org/10.1016/j.neucom.2017.06.053

Sun L, Shang Z, Xia Y, et al., 2020. Review of Bridge Structural Health Monitoring Aided by Big Data and Artificial Intelligence: From Condition Assessment to Damage Detection. *Journal of Structural Engineering*, 146(5), 04020073. https://doi.org/10.1061/(ASCE)ST.1943-541X.0002535

Sun M, Makki AM, and Kalhori H, 2017. Automated operational modal analysis of a cable-stayed bridge. *Journal of Bridge Engineering*, 22(12), 5017012. https://doi.org/10.1061/(ASCE)BE.1943-5592.0001141

Wu WH, Wang SW, Chen CC, et al., 2019. Modal parameter identification for closely spaced modes of civil structures based on an upgraded stochastic subspace methodology. *Structure and Infrastructure Engineering*, 15(3), 296–313. https://doi.org/10.1080/15732479.2018.1547770

Wu Y, Fu H, Bian X, et al., 2023. Impact of extreme climate and train traffic loads on the performance of high-speed railway geotechnical infrastructures. *Journal of Zhejiang University-SCIENCE A (Applied Physics & Engineering)*, 24(3), 189–205. https://doi.org/10.1631/jzus.A2200341

Yaghoubi V, Vakilzadeh M K, and Abrahamsson TJ, 2018. Automated modal parameter estimation using correlation analysis and bootstrap sampling. *Mechanical Systems and Signal Processing*, 100, 289–310. https://doi.org/10.1016/j.ymssp.2017.07.004

Yun CB, Cho S, Park HJ, et al., 2014. Smart wireless sensing and assessment for civil infrastructure. *Structure and Infrastructure Engineering*, 10(4), 534–550.

Zeng J, and Hu Z, 2022. Automated operational modal analysis using variational Gaussian mixture model. *Engineering Structures*, 273, 115139. https://doi.org/10.1016/j.engstruct.2022.115139

Electronic supplementary materials

Section S1

中文概要

题　目： 基于 OPTICS-KNN 聚类的两阶段自动模态参数识别方法

作　者： 陈轶[1,2], 傅文炜[3,4], 罗尧治[1], 沈雁彬[1,4], 杨晖[2], 汪士应[5]

机　构： [1]浙江大学，建筑工程学院，中国杭州，310058；[2]浙江交工集团股份有限公司，中国杭州，310051；[3]苏州科技大学，土木工程学院，中国苏州，215009；[4]浙江大学长三角智慧绿洲研究中心，未来城市实验室，中国嘉兴，314100；[5]杭州市交通规划设计研究院有限公司，中国杭州，310058

目　的： 自动化工作模态分析（AOMA）能够有效替代依赖人工干预和工程经验判断的传统模态参数识别方法。本研究提出一种融合协方差驱动随机子空间识别、稳定图自动判读及 OPTICS-KNN 自适应聚类策略的自动化模态识别框架，有效解决了传统模态参数识别方法的局限性。通过十层剪切框架数值模型和斜拉桥实测数据验证，该方法实现了高精度模态参数自动识别，具备应用于复杂工程结构实时监测的潜力。

创新点： 1. 采用两种广泛应用的模态验证准则对稳定图进行预处理，以消除部分虚假模态并提高聚类阶段的计算效率；2. 通过 k 近邻算法（KNN）确定最优聚类数量，并基于 OPTICS 算法实现自动化真实模态聚类。

方　法： 1. 采用协方差驱动随机子空间识别实现结构模态参数提取；2. 基于软硬准则开展稳定图的自动化初筛；3. 结合 OPTICS 算法与 k-近邻算法实现自适应物理模态聚类。

结　论： 1. 根据十层框架结构与桃夭门大桥的模态参数识别结果，结构的各阶模态频率与阻尼比均保持较小波动范围，表明该方法能有效剔除虚假模态并准确识别真实模态。2. 该方法对密集模态具有良好辨识能力，在无需预先设定聚类数量或设定聚类阈值的情况下，成功实现了此类模态的精准识别。3. 通过对桃夭门大桥的监测数据进行分析，进一步验证了该方法在工程实践中的实用性。

关键词： 结构健康监测；基于协方差驱动随机子空间识别；自动工作模态分析；OPTICS；K-近邻算法